Danuta PLIŚ, Jadwiga PŁOSZYŃSKA

Department of Electrodynamics and Electrical Machine Systems, Rzeszów University of Technology

The effect of relative magnetic permeability of wedges closing stator slots in a cage induction motor on rotor cage heating during the starting phase

Streszczenie. *Opracowanie algorytmu obliczeń elektromagnetycznych silnika indukcyjnego klatkowego z klinami magnetycznymi w powiązaniu z obliczeniami termicznymi, stworzyło możliwości porównania wpływu względnej przenikalności magnetycznej μ_{rk} na nagrzewanie się prętów klatki wirnika. Zastosowanie klinów magnetycznych powoduje uzyskanie wyższej temperatury uzwojenia wirnika, lecz proces nagrzewania przebiega wolniej, a rozkład temperatury jest bardziej równomierne.*

Abstract*. By developing an algorithm for electromagnetic calculations of parameters characterizing a cage induction motor equipped with magnetic wedges in connection with thermal calculations it became possible to compare the effect of the relative magnetic permeability μ_{rk} on rotor cage bars heating process. The use of magnetic wedges results in reaching a higher rotor winding temperature, but the heating proceeds slower and the temperature distribution is more uniform.* (***Wpływ względnej przenikalności magnetycznej klinów zamykajqcych żłobki stojana na nagrzewanie się klatki wirnika w czasie rozruchu silnika indukcyjnego klatkowego***).

Słowa kluczowe: kliny magnetyczne, silniki indukcyjne, nagrzewanie uzwojeń, rozkład temperatury.
Keywords: magnetic wedges, induction motors, winding heating, temperature distribution.

Introduction

The requirements that are nowadays expected to be met by high-voltage induction motors in the area of energy efficiency, noise, vibration and reduction of parasitic effects, generate a need for detailed analysis of these phenomena. This is in turn related to the necessity to carry out an analysis of the slot-adjacent zone of the core, including the appropriateness of the use of magnetic wedges to close stator slots in cage induction motors, as well as slots in stators and rotors of slip-ring induction motors. Where motors are powered by converter systems, the above-listed issues must include also consideration aimed at assessment of advisability and optimum selection of magnetic wedges. By replacing non-magnetic wedges closing the slots with magnetic ones, it is possible to influence the slot conductivity, teeth saturation state in the slot-adjacent zone, and the Carter's coefficient value. The changes are related to achieving other electromagnetic parameters affecting static properties of motors [1, 2, 3]. In the course of motor starting, presence of magnetic wedges has an effect on distribution of current density and losses in rotor windings and thus also on the bar heating process. In high-power induction motors, during prolonged starting phase or blockage of rotor, significant amounts of thermal energy are generated, especially in the rotor winding. An additional unfavourable phenomenon is an uneven distribution of temperature in the rotor winding volume and the related destructive mechanical stresses. To calculate distribution of the temperature field in the region adjacent to rotor bars with magnetic wedges used in an induction motor's stator, the cage winding transient heating analysis method was used. The effect of transient heating on electromagnetic parameters decisive for distribution of thermal losses in the winding region was taken into account.

The use of magnetic wedges has a positive effect on parameters related to the transient state, in particular the rated operating point. The analysis of the involved effects, both positive and negative ones, on the electromagnetic calculations stage may provide knowledge useful both in design work and manufacturing process.

Thermal model of the rotor cage

To calculate the temperature distribution inside a rotor bar, a thermal field model was used of an induction motor rotor's deep-slot winding described by means of the Fourier-Kirchhoff equation with appropriate boundary conditions and an initial condition. For bars with trapezoidal cross-section, analysis of transient thermal state was carried out in the system of polar co-ordinates [4]. The rotor winding and the surrounding medium constitute a complex thermal system. The largest temperature increase steepness should be expected primarily in the region of the bars' in-slot portion. The cross-section of a deep-slot winding with trapezoid-shaped bars was modelled by a ring segment with corresponding taper angle value, with width of the ring equalling the bar height. A difficulty in description of the deep-slot winding temperature field consists in inhomogeneous distribution of heat sources in the winding volume as well as uneven conditions of heat interception from its surface. The cause of such state lies in the environment surrounding the bar. In in-slot portion, distribution of sources is determined by the current displacement phenomenon, therefore this part of the winding is characterised by an uneven distribution of the sources, especially along the bar height. Heat interception in this area is of complex nature and occurs via the equivalent air gap to the pack of core laminations. It is described by means of a boundary condition that can be expressed in the form:

$$-q = \frac{\lambda_p}{\delta_p}(\theta - \theta_0), \tag{1}$$

where q denotes quantity of heat flowing through a body, λ_p — thermal conductivity of the air gap, δ_p — thickness of gap between the bar and the slot, θ — temperature, and θ_0 — initial temperature.

In the out-of-pack portion of bars and in closing rings, distribution of sources is a result of electromagnetic parameters varying with temperature. The heat flux density for surfaces remaining in contact with air in this portion of winding is described by the boundary condition of third type:

$$-q = \alpha(\theta - \theta_0), \tag{2}$$

where α is the thermal diffusivity of the medium.

A deep-slot winding is characterised with a large aspect ratio of cage bars. The temperature varies insignificantly along their width. This allows to assign some mean value to temperature along these dimensions and consider the thermal model in a two-dimensional system of co-ordinates. Bearing in mind that the rotor core has a laminar structure, thermal conductivity of the pack of laminations in axial direction is much less than this along the laminations. Thermal diffusivity of the core material (a) for ***z***-axis direction has therefore a different value (a_{zz}) than this for the radial co-ordinate ***r*** (a_z). In the light of remarks and assumptions made above, the transient thermal state in the cage winding and in the rotor core can be described by conductivity equations that in the system of polar co-ordinates for trapezoidal bars take the following forms:
— for the in-slot portion of bars,

$$\frac{\partial\theta_m}{\partial\tau} = a_m\left(\frac{\partial^2\theta_m}{\partial r^2}+\frac{1}{r}\frac{\partial\theta_m}{\partial r}+\frac{\partial^2\theta_m}{\partial z^2}\right)- \\ -\frac{1}{r}\frac{2\lambda_p}{c_m\rho_m\gamma\delta_p}\left(\theta_m-\theta_z\right)+\frac{q_{vm}(r,z,\tau)}{c_m\rho_m} \quad \text{(3a)}$$

— for the out-of-pack portion of bars,

$$\frac{\partial\theta_m}{\partial\tau} = a_m\left(\frac{\partial^2\theta_m}{\partial r^2}+\frac{1}{r}\frac{\partial\theta_m}{\partial r}+\frac{\partial^2\theta_m}{\partial z^2}\right)- \\ -\frac{1}{r}\frac{2\alpha_m}{c_m\rho_m\gamma}\left(\theta_m-\theta_0\right)+\frac{q_{vm}(r,z,\tau)}{c_m\rho_m} \quad \text{(3b)}$$

— for the closing ring,

$$\frac{\partial\theta_m}{\partial\tau} = a_m\left(\frac{\partial^2\theta_m}{\partial r^2}+\frac{1}{r}\frac{\partial\theta_m}{\partial r}+\frac{\partial^2\theta_m}{\partial z^2}\right)+ \\ +\frac{q_{vm}(r,z,\tau)}{c_m\rho_m} \quad \text{(3c)}$$

— for the teeth laminations pack,

$$\frac{\partial\theta_z}{\partial\tau} = a_z\left(\frac{\partial^2\theta_z}{\partial r^2}+\frac{1}{r}\frac{\partial\theta_z}{\partial r}\right)+a_{zz}\left(\frac{\partial^2\theta_z}{\partial z^2}\right)+ \\ +\frac{1}{r}\frac{2\lambda_p}{c_z\rho_z\beta\delta_p}\left(\theta_m-\theta_z\right)+\frac{q_{vz}}{c_z\rho_z} \quad \text{(3d)}$$

where c denotes the specific heat of the material, ρ — material density, q_v — power losses per unit volume, γ — ring segment taper angle, and β — equivalent taper angle of the laminations pack segment.

Distribution of internal heat sources occurring in equations (3a–c) depends on varying temperature, position and a transient electromechanical process proceeding in the course of motor starting. Determination of the temperature field in electromechanically transient conditions requires therefore to link the solution of conductivity equations with the solution of the dynamic equation of motion. To take the phenomena into account, the elementary conductors method [4] was used to determine thermal losses.

Calculation of motor characteristics as time functions

Calculations are carried out from $\tau = 0$ s to the end of starting phase, with time τ increasing discretely with an assumed step. For each point of the characteristics (moment in time), calculations are carried out according to the algorithm shown in Fig. 1 and with the use of adopted procedures: solving the motor's substitution scheme, calculating current displacement, calculating temperature distribution in the rotor bar, and calculating the effect of temperature and saturation on the parameters. The circuit-field method was applied in the calculations. Field-related calculations pertain to temperature and magnetic field distribution in vicinity of the slot. To solve the adopted mathematical model, numerical methods were applied [1, 5]. Results obtained from the calculations were used in solving the equivalent diagram with temperature-induced variation of parameters and degree of saturation taken into account.

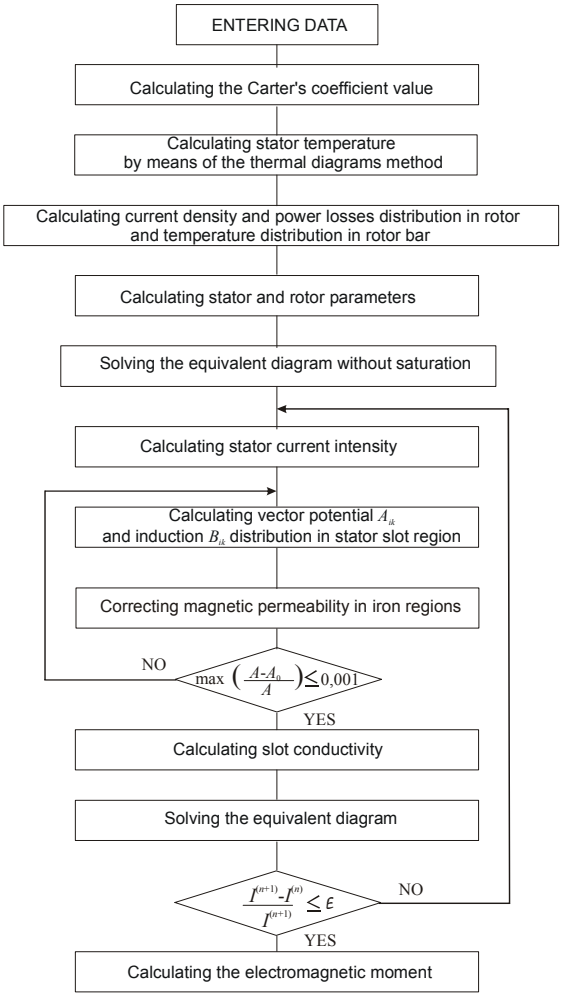

Fig. 1. Algorithm used for calculations of induction motor characteristics

Calculation results

Simulation studies were carried out for SZJC 196T EX 6 kV/320 kW induction three-phase induction motor. In the stator, rectangular slots were modelled closed with magnetic wedges with relative magnetic permeability $\mu_{rk} = 3$ and $\mu_{rk} = 5$. Analysis of the electromagnetic moment, stator current intensity and rotor cage temperature increase at the assumed values of the wedge's relative magnetic permeability μ_{rk} in the stator was performed within the velocity ranging from zero to the determined rated load moment value. Figs. 2(a) and 2(b) show waveforms of the electromagnetic moment and the stator current intensity in the course of motor starting phase, with different values of the wedge's relative magnetic permeability μ_{rk} taken into account.

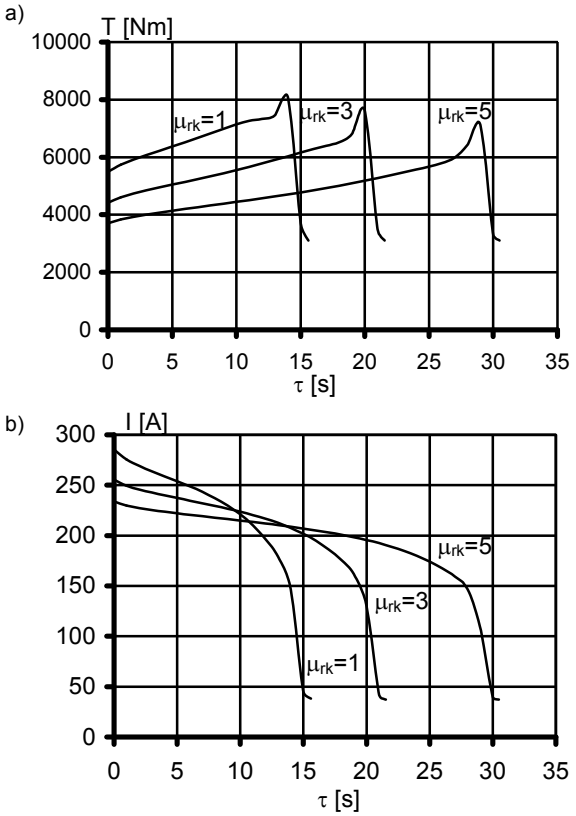

Fig. 2. Calculated waveforms of: (a) electromagnetic moment, (b) stator current intensity during starting phase of SZJC 196T EX 6 kV 320 kW motor with magnetic wedges in the stator (μ_{rk} = 3; 5) compared to the current intensity waveform of the motor with non-magnetic wedges (μ_{rk} = 1) and with the effect of temperature on resistivity in the course of starting taken into account

The obtained results concerning the rotor cage heating for different values of the stator wedges' relative magnetic permeability μ_{rk} are presented in the form of plots representing distribution of temperature along the bar height in its in-slot portion (A), out-of-slot portion (B) and in the closing ring (C). Below, the following cases are presented graphically: the maximum temperature difference occurring between upper and lower face of a bar in its in-slot portion (Figs. 3(a)–(c)); temperature of the bar in the in-slot region reaching a maximum value (Figs. 4(a)–(c)); thermal state reached after the end of the starting phase (Figs. 5(a)–(c)).

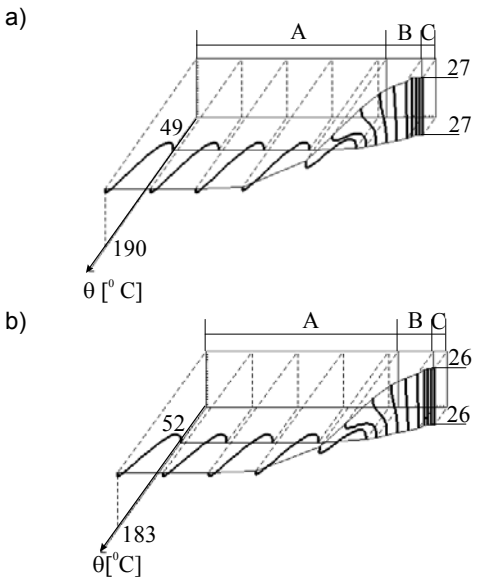

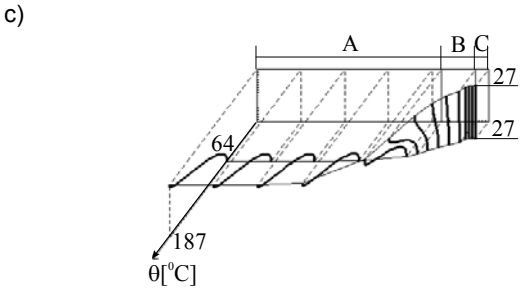

Fig. 3. Thermal state of the rotor cage at time τ corresponding to the largest temperature difference between the upper and the lower face of the bar's in-slot portion in a motor with wedges with the relative magnetic permeability μ_{rk} in the stator
(a) τ = 6 s, μ_{rk} = 1; (b) τ = 7 s, μ_{rk} = 3; (c) τ = 9 s, μ_{rk} = 5

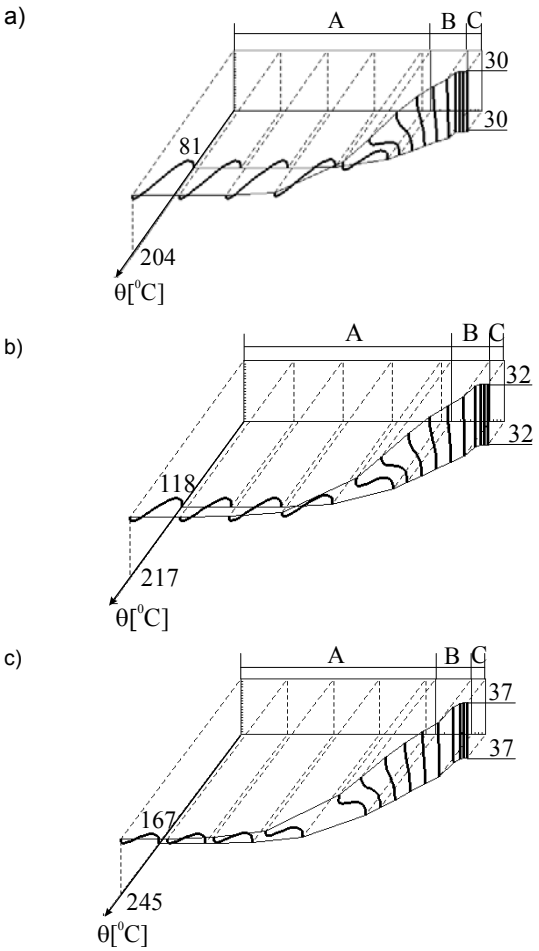

Fig. 4. Thermal state of the rotor cage at time τ corresponding to the largest temperature in the bar's in-slot portion in a motor with wedges with the relative magnetic permeability μ_{rk} in the stator
(a) τ = 9 s, μ_{rk} = 1; (b) τ = 14 s, μ_{rk} = 3; (c) τ = 22 s, μ_{rk} = 5

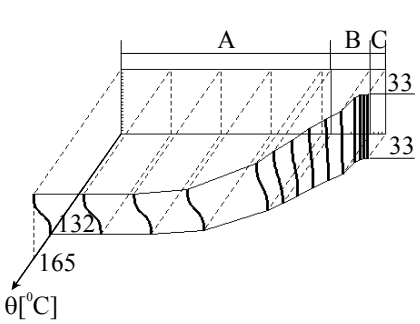

b)

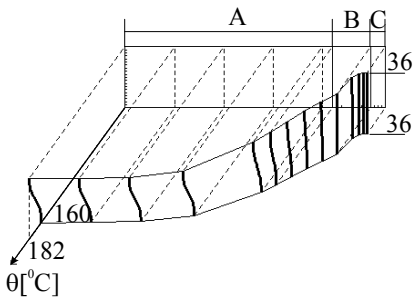

c)

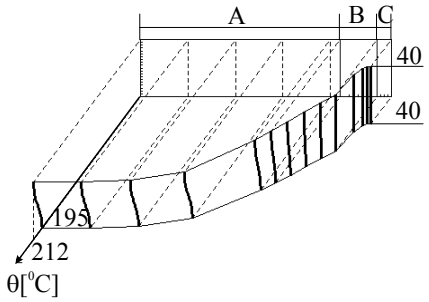

Fig. 5. Thermal state of the rotor cage at time τ (after the starting phase end) in a motor with wedges with relative magnetic permeability μ_{rk} in the stator
(a) τ = 15.6 s, μ_{rk} = 1; (b) τ = 21.5 s, μ_{rk} = 3; (c) τ = 30.5 s, μ_{rk} = 5

Fig. 6 shows plots representing heating of lower and upper layer of a bar at central point of its length.

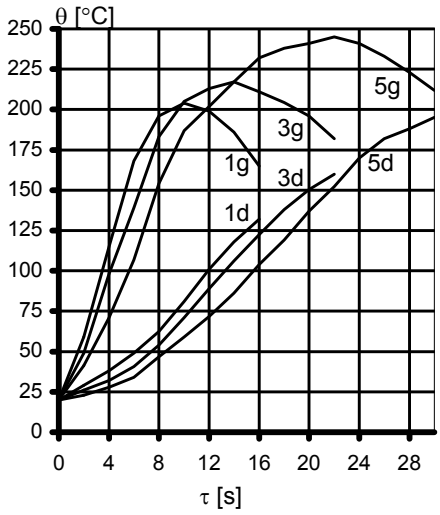

Fig. 6. The plot representing heating of a bar at upper (g) and lower (d) layer of its central in-slot point: 1g, 1d — for non-magnetic wedges; 3g, 3d — for wedges with μ_{rk} = 3; 5g, 5d — for wedges with μ_{rk} = 5

Conclusion

Rotor cage bars in motors with magnetic wedges heat up more evenly compared to bars in motors with non-magnetic wedges. The largest difference between temperature of the rotor cage bar's upper and lower face in its in-slot portion is $\Delta\theta$ = 141°C for the motor with non-magnetic wedges, compared to $\Delta\theta$ = 131°C in a motor with magnetic wedges characterised by the relative magnetic permeability μ_{rk} = 3 and $\Delta\theta$ = 123°C for wedges with μ_{rk} = 5. In a motor with non-magnetic wedges, the in-slot portion of cage bar reaches its maximum temperature of θ = 204°C after 57% of the starting period, compared to the maximum bar temperature of θ = 217°C reached after 65% of the starting period in a motor with magnetic wedges characterised with magnetic permeability of μ_{rk} = 3 and θ = 245°C observed after 72% of the starting period in a motor with wedges with μ_{rk} = 5. After the end of the starting phase, the rotor cage bar in motor with non-magnetic wedges has reached temperature θ = 165°C in its in-slot portion, compared to θ = 182°C in motor with magnetic wedges with relative magnetic permeability μ_{rk} = 3 and θ = 212°C for wedges with relative magnetic permeability μ_{rk} = 5.

REFERENCES

[1] Pliś D., Wpływ klinów magnetycznych na parametry elektromechaniczne maszyn elektrycznych prądu zmiennego (*The effect of magnetic wedges on electromechanical parameters of AC electric machines*, in Polish), PhD Thesis, Gliwice 2002

[2] Pliś D., Badania symulacyjne silników z klinami magnetycznymi (*Simulation studies on motors with magnetic wedges*, in Polish), *Przegląd Elektrotechniczny,* 12 (2004), 1258–1261

[3] Płoszyńska J., Rut R., Pliś D., Analiza parametrów elektromechanicznych ustalonego punktu pracy silnika indukcyjnego o żłobkach zamkniętych materiałem magnetycznym (*An analysis of electromechanical parameters at the stationary working point of a motor with slots closed with a megnetic material*, in Polish), *Zeszyty Problemowe BOBRME Komel*, 64 (2002), 105–109

[4] Rut R., Płoszyńska J., Analiza stromości narastania temperatury w uzwojeniach klatkowych wysokonapięciowych silników indukcyjnych dużej mocy (*An analysis of the temperature increase steepness in cage windings of high-power induction motors*, in Polish), *Prace Naukowe Instytutu Maszyn, Napędów i Pomiarów Elektrycznych Politechniki Wrocławskiej*, 48 (2000), 77–85

[5] Pliś D., Model obwodu magnetycznego silnika indukcyjnego z klinem magnetycznym (*A magnetic circuit model for induction motor with magnetic wedge*, in Polish), *Przegląd Elektrotechniczny,* 12 (2003), 912–915

Authors: *Danuta Pliś, Eng., DSc, Faculty of Electrical & Computer Engineering, Rzeszów University of Technology, ul. W. Pola 2, 35-959 Rzeszów, Poland, e-mail: dplis@prz.edu.pl; Jadwiga Płoszyńska, Eng., DSc, Faculty of Electrical & Computer Engineering, Rzeszów University of Technology, ul. W. Pola 2, 35-959 Rzeszów, Poland, e-mail: jadplo@prz.edu.pl.*